Journal of Materials Chemistry A

Accepted Manuscript

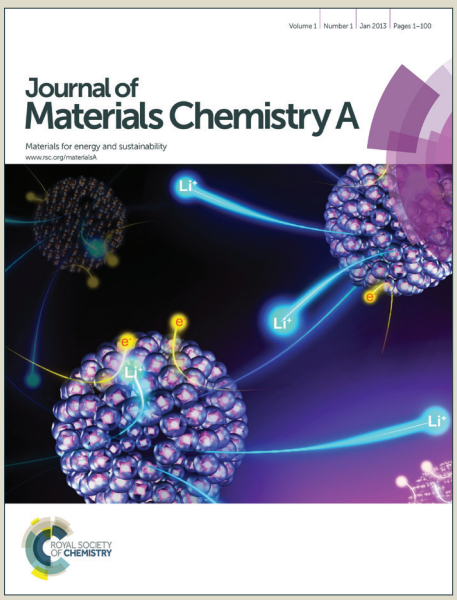

ROYAL SOCIETY OF CHEMISTRY

www.rsc.org/materialsA

Journal Name

ARTICLE

One-step synthesis of nanorod-aggregated functional hierarchical iron-containing MFI zeolite microspheres

Received 00th January 20xx,
Accepted 00th January 20xx

DOI: 10.1039/x0xx00000x

www.rsc.org/

Weigang Li[a], Gang Li*[a], Changzi Jin[b], Xin Liu[b], Junhu Wang[b]

A novel hierarchical iron-containing MFI zeolite microsphere composed of oriented-assembled nanorods was prepared through one-step hydrothermal crystallization without mesoporous template agent. Meanwhile, this is the first report on constructing functional hierarchical zeolite microsphere with aggregated MFI nanorods and well-dispersed α-Fe_2O_3 nanoparticles by adding glucose into the synthetic system. The obtained samples were characterized by powder XRD, N_2 physical adsorption-desorption, FT-IR spectra, UV-Vis spectra, XPS spectra and Mössbauer spectra. The results show that the microspheres possess uniform diameters from 4 to 5μm, hierarchical porous structure, high surface area (502 m^2 g^{-1}) and well-dispersed ultrafine α-Fe_2O_3 nanoparticles. More importantly, the microspheres had been proven to have excellent catalytic performance for photocatalytic degradation of phenol. Thus, this synthesis method opens up routes for the in-situ preparation of other functional porous materials with unique nanostructure.

Introduction

Zeolites have been widely used in the field of catalysis, separation, ion-exchange and adsorption due to their uniform pore sizes, large internal surface area, intrinsic chemical activity and high thermal stability.[1-6] However, the microporous channel of zeolites strongly inhibit the diffusion of reactants, especially for bulkier molecules, thus eliminating the mass transport limitation is urgently solved. Using nano-zeolite is a good way to get faster diffusion rate of reactants and products. But, it is inconvenient to directly use nano-zeolites in practical applications because of the difficulty in recycling them after reaction. Zeolite microspheres aggregated of nanocrystals with a hierarchical porosity is an excellent candidate to overcome this problem. Up to now, several similar microspheres have been synthesized by different methods.[7-14] For example, Sterte et al.[7, 8] prepared zeolite microspheres by a method based on the use of anion exchange resins as shape-directing macro-templates. Tang et al.[9] applied the polymerization-induced colloid aggregation method to assemble zeolite nanocrystals into microspheres. Han et al.[10] applied pluronic triblock copolymer (F127) to prepare zeolite microspheres with macro-porosity. Shi et al.[11] used poly-(methyl methacrylate) (PMMA) as a dual-functional template to prepare mesoporous zeolite microspheres. Recently, Wang et al.[12] obtained hierarchical MFI zeolite microspheres through the hydrothermal crystallization of a carbon-silica composite monolith. Although porous microspheres have been prepared in various ways as introduced above, these methods usually need complex multi-step synthesis route or variety of polymer and surfactant as shape-directing agents.

Expanding the scope from pure zeolites to hybrid materials, by combining the properties of zeolites with other functional components (e.g., iron), significantly broadens the field of zeolite material capability.[15-18] Part of the materials can be used to treat waste water as heterogeneous Fenton-like catalyst. Conventionally, iron ions are introduced into zeolite using the post-processing methods such as impregnation processes. It is worth noting that these generated functional components deposited on the surface are typically too big or not well-dispersed throughout the zeolites, resulting in easy desquamation from zeolite and loss of function. In situ crystallization approach is an ideal method to prepare functional zeolite. Nevertheless, it is very difficult to simultaneously control the growth of zeolites and the properties of the functional components in terms of particle size and dispersion.[15, 19, 20] Thus, how to use a flexible method for synthesis of functional hierarchical zeolite microspheres is a huge challenge.

In this paper, we provide a flexible and simple processing method first employed to prepare hierarchical iron-containing MFI zeolite microspheres. The functional zeolite microspheres with hierarchical porous structure, high surface area and well-dispersed ultrafine α-Fe_2O_3 nanoparticles are prepared by adding glucose into the synthetic system. The synthesis route of microspheres is shown in Scheme 1. In particular, the obtained functional microspheres are investigated as hetero-geneous Fenton-like catalyst for photocatalytic degradation of phenol and show excellent catalytic performance.

[a] State Key Laboratory of Fine Chemicals, School of Chemical Engineering, Dalian University of Technology, Dalian 116024, China.
[b] Mössbauer Effect Data Center & Laboratory of Catalysis and New Materials for Aerospace, Dalian Institute of Chemical Physics, Chinese Academy of Sciences, Dalian,116023 China.

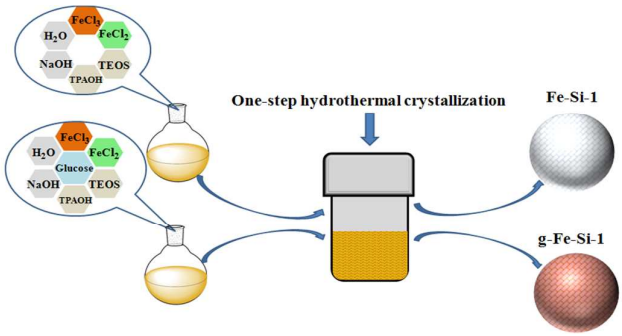

Scheme 1. The synthesis route of microspheres

Experimental

Chemicals

Tetraethyl orthosilicate (TEOS), tetrapropylammonium hydroxide (TPAOH, 1M), Iron(III) chloride hexahydrate, Iron(II) chloride tetrahydrate, sodium hydroxide, glucose, phenol and H_2O_2 (30 wt.%) were bought from Tianjin Kermel Chemical Co. All reagents were used as received without further purification.

Synthesis of zeolite microspheres

The typical synthesis process of hierarchical Fe-Si-1 microspheres was as follows. 19 ml TPAOH (1M) was added to a mixed solution containing 16.5 g TEOS, 1 g Iron (III) chloride hexahydrate, 0.4 g Iron (II) chloride tetrahydrate and 44.5 ml of distilled water under vigorous stirring at 35 °C. After stirring for 3 h, 26 ml NaOH aqueous solution (1M) was added to above gel mixture to adjust pH value. After further stirring for 6 h at room temperature, the gel mixture was transferred to a Teflon-lined stainless-steel autoclave and heated at 170 °C for 3 days. The product was filtrated, dried, and calcined in air at 550 °C for 6 h to remove the templates. Finally the Fe-Si-1 microspheres were obtained. Hierarchical g-Fe-Si-1 microspheres were prepared using the same procedure as described above except for adding glucose. The sample was designated as g-Fe-Si-1(x), where x (1-4 g) is the content of glucose.

Characterization

Powder XRD patterns were recorded on a Rigaku D/Max 2400 diffractometer using Cu Kα radiation (40 kV and 40 mA). The nitrogen adsorption and desorption isotherm was measured at -196°C using a Quantachrome AUTOSORB-1 physical adsorption apparatus. The specific surface area and pore-size distribution were calculated by using the Brunauer-Emmett-Teller (BET) method and Barrett-Joyner-Halenda (BJH) adsorption model, respectively. FT-IR and UV-Vis spectroscopy were employed to identify the solid powder samples. FT-IR spectra were recorded on a Bruker EQUINOX55 spectrometer, using KBr pellet technique. UV-Vis spectra were measured on a Jasco UV-550 spectrophotometer. SEM images were collected on a FEI Quanta 450. XPS was conducted to determine the states of iron in material using a Thermo ESCALAB 250 X-ray photoelectron spectrometer. Al-Kα acted as light source and Cls (284.6 eV) was used to correct XPS peaks of other elements. The ^{57}Fe Mössbauer spectra were recorded using a Topologic 500A spectrometer and a proportional counter at room temperature. ^{57}Co (Rh) moving in a constant acceleration mode was used as radioactive source. The iron content of samples was measured by an Optima 2000 DV Inductively Coupled Plasma optical emission spectrometer (ICP/OES).

Catalytic reaction

The zeolite microspheres were used as heterogeneous Fenton-like catalyst for photocatalytic degradation of phenol. The reaction suspension was prepared by adding catalyst (0.2 g) into aqueous solution of phenol (200.0 mL, 500.0 mg L^{-1}) and stirred for 30 min to ensure an adsorption-desorption equilibrium. H_2SO_4 (0.1 mol L^{-1}) was added gradually to adjust the pH value. After that, H_2O_2 (30 wt. %, 1.0 mL) was introduced into above suspension. At the same time, UV light was turned on and this was considered as the initial time for reaction. The temperature of reaction suspension was maintained at 25 °C by cooling water circulation. Samples were taken out from the reaction suspension after various reaction times to analyze chemical oxygen demand (COD) with potassium dichromate method. The samples and excessive potassium dichromate standard solution were added in sulfuric acid solution, and then the organic species in the samples were oxidized by microwave digestion. The excessive potassium dichromate was quantitated by reversing-titration method with ammonium ferrous sulfate standard solution. Lastly, COD was calculated according to the consumption of ammonium ferrous sulfate. For the recyclability tests, the catalyst after reaction was recovered by centrifugation and washed with deionized water several times, then reused in the next run under the same reaction condition.

Results and discussion

Characterizations of material

The SEM images of Fe-Si-1 and g-Fe-Si-1(x) after combustion of templates are presented in Fig. 1. As shown in the SEM images, the Fe-Si-1 is composed of relatively uniform spherical particles of 4-5 μm in diameter. The SEM image (Fig. 1c) clearly indicates that the obtained microspheres are composed of nanorods 100-200 nm in width, which self-assembles into the intact spherical morphology of the product. It is interesting to note that g-Fe-Si-1(2) (Fig. 1 g-i) maintains the nanorod-aggregated spherical morphology. However, the morphology of g-Fe-Si-1(4) (Fig. 1 m-o) obviously changes into the archetype MFI morphology, which often described as twinned prisms. At the same time, there is a large amount of amorphous material in the sample. The results suggest that glucose has much influence on the morphology of the product. Adding a small amount of glucose in this system (see Experimental Section for details) will not destroy the spherical structure, but the morphology of the product will transform as

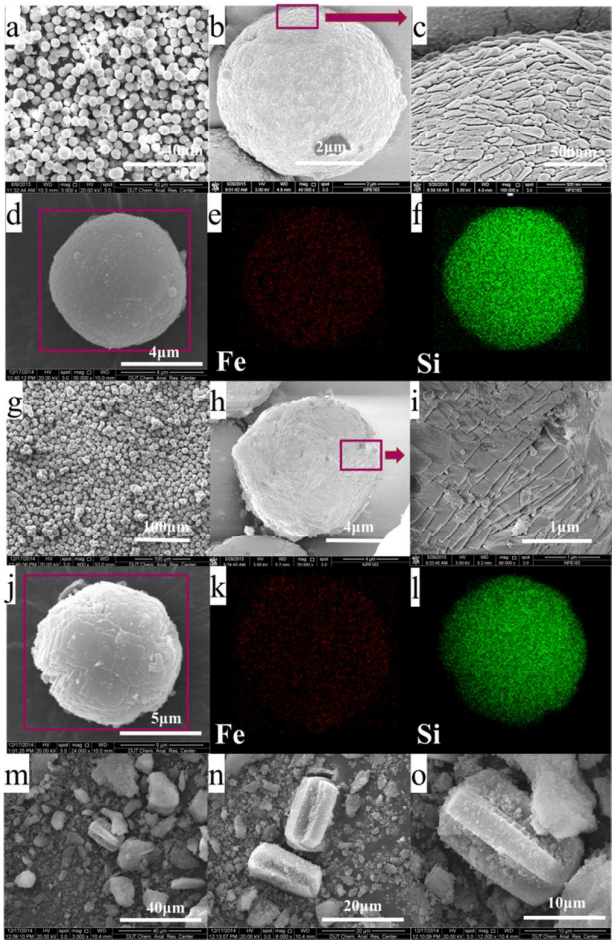

Fig.1 SEM images of (a-f) calcined Fe-Si-1 and its EDX elemental maps of Fe and Si; (g-l) calcined g-Fe-Si-1(2) and its EDX elemental maps of Fe and Si; (m-o) calcined g-Fe-Si-1(4)

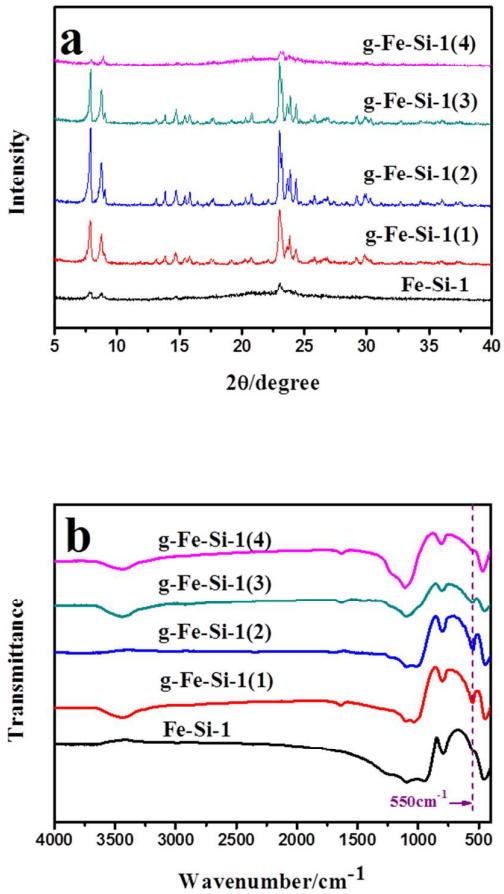

Fig. 2 XRD pattern (a) and FT-IR spectra (b) of Fe-Si-1, g-Fe-Si-1(1), g-Fe-Si-1(2), g-Fe-Si-1(3) and g-Fe-Si-1(4)

the further addition of glucose. The SEM images of Fe-Si-1 and g-Fe-Si-1(2) microsphere sample, combined with EDX elemental mappings (Fig. 1d-f, j-l), show that the iron species are uniformly dispersed throughout the sample and the iron contents are 7.13 and 6.11wt%, respectively. Besides, the iron contents of Fe-Si-1 and g-Fe-Si-1(2), which were determined by inductive coupled plasma optical emission spectroscopy, are 6.89 and 6.99 wt%, respectively. The differences between two samples are relatively small, which demonstrates that the glucose have no influence on leaching of iron ion from zeolite.

The XRD patterns of the calcined samples are shown in Fig. 2a. All the samples exhibit the characteristic diffraction peaks occurred at 2θ of 8.01° , 8.91° ,23.21° , 24.01° , and 24.51 ° , which coincides very well with MFI structure materials, and no typical diffraction peaks due to iron oxide aggregates are found. Obviously, the crystallinity of the samples increased firstly and then decreased with increasing the amount of glucose. The samples were further characterized by FT-IR spectra (Fig. 2b). Besides two typical bands at 805 and 450 cm^{-1} ascribed to symmetry stretch and bend stretch of Si-O in the SiO_4 units,[21] all samples present a band at 550 cm^{-1}, which is usually assigned to the double five rings of the characteristic structure of MFI-type zeolites and is another mean to characterize the crystallinity of this kind of zeolites,[22, 23] g-Fe-Si-1(2) possesses the strongest 550 cm^{-1} peak, while the peak is very weak for Fe-Si-1 or g-Fe-Si-1(4). It can be seen that the change of the peak intensity at 550 cm^{-1} is corresponded with that of crystallinity obtained from XRD patterns. The results demonstrate that the content of glucose in the synthetic system shows strong influence on the crystallization of zeolite.

N_2 adsorption-desorption experiments were performed to determine the textural properties of Fe-Si-1 and g-Fe-Si-1(2). The adsorption isotherms (Fig.3a, b) exhibit a hysteresis loop at higher relative pressures, indicating the microspheres contain larger pore beside intrinsic micropore. The pore diameter distribution curve derived from the BJH model displays a clear secondary porosity with a diameter 3.7 nm (shown in Fig. 3 inset), suggesting that the nanorod in the microspheres are not packed very tightly. The mesopores is believed to favor the diffusion of larger molecules. On the other hand, the glucose does not play the role of mesopores

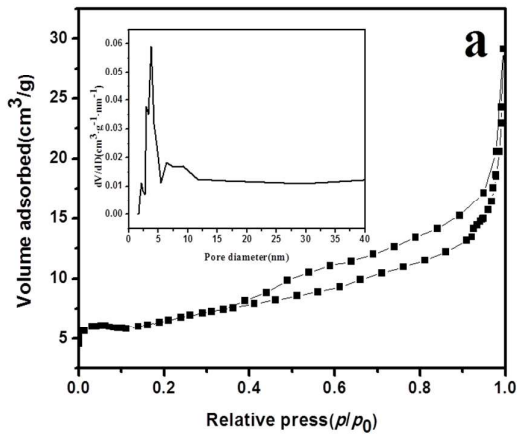

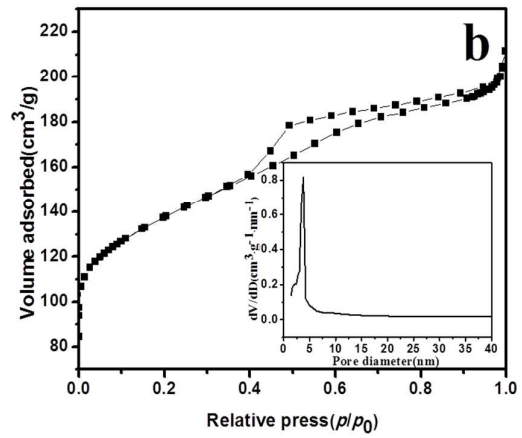

Fig. 3 N_2 sorption isotherm and mesoporous pore size distribution (inset) of (a) Fe-Si-1 and (b) g-Fe-Si-1(2)

template as Fe-Si-1 and g-Fe-Si-1(2) possess the same pore diameter distribution. The BET surface area of Fe-Si-1 and g-Fe-Si-1(2) are calculated to be 23 m^2 g^{-1} and 502 m^2 g^{-1}, respectively. The huge distinction in the surface area for the two samples is attributed to the difference of crystallinity.

The coordination state and extent of aggregation of Iron species in the iron-containing zeolites are investigated by UV–Vis spectroscopy (Fig. 4). The spectrum of Fe-Si-1 are dominated by the intense Fe-O charge transfer band below 250 nm related to isolated tetrahedral Fe species, which are in or out the zeolite framework. It also displays a band around 290 nm, which is due to highly dispersed, possibly isolated Fe^{3+} complexes at extra-framework positions. In previous research, the bands at 333 and 427 nm are ascribed to Fe^{3+} oligomeric clusters.[24-27] While for Fe-Si-1, the two bands shifted slightly to 375 and 440 nm, which may be induced with the increase of the cluster size after most severe thermal treatments. The spectrum of g-Fe-Si-1(2) shows wide range of Fe-O charge

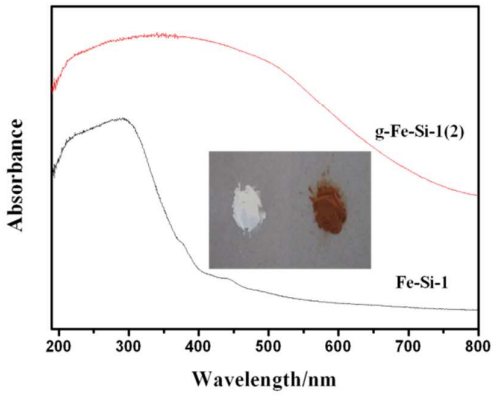

Fig. 4 UV-Vis spectra of Fe-Si-1 and g-Fe-Si-1(2), insert: the pictures of (left) Fe-Si-1 and (right) g-Fe-Si-1(2) powder samples

transfer bands in the range of 210-500 nm, which is ascribed to iron oxide.[28,29] Owing to overlap with the peak, other bands of Fe species can't be seen in the spectrum. Inset of Fig. 4 shows that the colors of Fe-Si-1 and g-Fe-Si-1(2) are white and brick red, respectively. Thus, all the results clearly indicate that the Fe species undergo tremendous changes after adding glucose.

XPS is used to examine the local oxidation states and chemical bonding environment of the material. XPS narrow region scans of Fe 2p in Fe-Si-1 and g-Fe-Si-1(2) are shown in Fig. 5. Two peaks located approximately 712 and 725 eV, corresponding to Fe $2p_{3/2}$ and Fe $2p_{1/2}$, respectively, are clearly seen in the spectra. The Fe 2p region of the XPS spectrum is complex and often includes contributions from overlapping peaks of Fe^0, Fe^{2+} and Fe^{3+} oxides. The signals of Fe-Si-1 are very weak, indicating that most of iron species is located inside the microspheres instead on the external surface. The XPS results reveal that only framework or extra-framework Fe^{3+} exist in the microspheres of Fe-Si-1, and there is no obvious change after being calcined. However, for the sample g-Fe-Si-1(2) (Fig.5(c)), it can be noted that two peaks at 710 and 712 eV are displayed, corresponding to the Fe $2p_{3/2}$ peak for FeO and α-Fe_2O_3.[30-32] These demonstrate that Fe^{2+} is prevented transforming to Fe^{3+} with the adding of glucose that has the strong reducing capability, and the Fe^{3+} species partially trend to form α-Fe_2O_3 simultaneously. In the XPS spectrum of calcined g-Fe-Si-1(2) (Fig.5 (d)), the peak of FeO disappears, indicating that FeO is oxidized to α-Fe_2O_3 after calcination at high temperature.

A series of Mössbauer spectra of as-prepared or calcined Fe-Si-1 and g-Fe-Si-1 are shown in Fig. 6 and corresponding data extracted from the fits are collected in table 1. In the Mössbauer spectra, the isomer shift (IS) and quadrupole splitting (QS) reflect the valence state and coordination of the high spin Fe^{3+} and Fe^{2+} complexes, respectively. [33-36] In oxygen-coordinated compounds, states with IS<0.3 mm/s at room temperature are usually assigned to Fe^{3+} in tetrahedral coordination (Fe^{3+}_{Th}), while those with IS>0.3 mm/s are assigned

Journal Name

ARTICLE

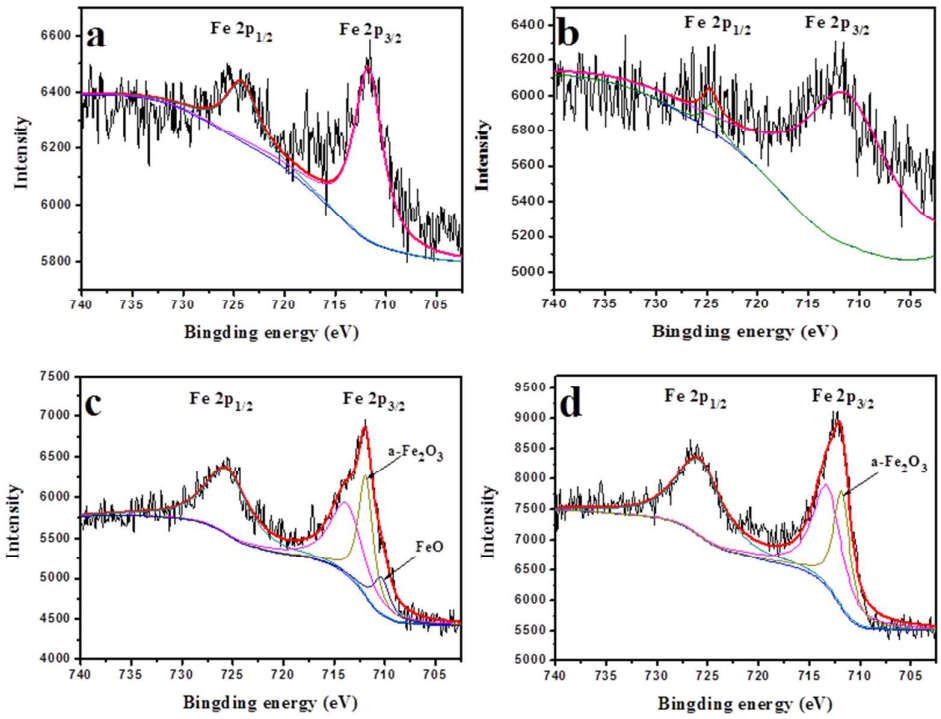

Fig. 5 XPS spectra of Fe $2p_{3/2}$ and Fe $2p_{1/2}$ regions for (a) as-prepared Fe-Si-1, (b) calcined Fe-Si-1, (c) as-prepared g-Fe-Si-1(2) and (d) calcined g-Fe-Si-1(2)

to octahedral coordination (Fe^{3+}_{Oh}). Fe^{2+} ions with coordination numbers 5 and 6 are characterized by the higher values of the following parameters: IS=1.1-1.3 mm/s, QS>1.5 mm/s.[37-41] The Mössbauer spectra of as-prepared Fe-Si-1 is deconvoluted into two components (A1 and A2) and the IS values of 0.34 and 0.38 mm/s correspond to the presence of Fe^{3+}_{Oh}. After being calcined, the components of Fe-Si-1 are B1 (IS=0.26 mm/s) and B2 (IS=0.22 mm/s), which are attributed to Fe^{3+}_{Th}. The results reveal the components represent octahedral lattice iron atoms upon hydration, and these are reversibly transformed into tetrahedral iron species upon dehydration. On the other hand, the calcination process induces partial Fe^{3+} migration from framework toward extra-framework positions with formation of Fe^{3+} oligomeric clusters. According to the above analysis results, we assigned the A1 and B1 components to framework Fe species, the A2 and B2 to extra-framework Fe species.[42] For the sample as-prepared g-Fe-Si-1(2), the high IS and QS value of the C1 component (IS= 1.28 mm/s, QS= 2.37 mm/s) indicates the presence of Fe^{2+}, but the signal disappears in calcined g-Fe-Si-1(2), suggesting that Fe^{2+} is oxidized to Fe^{3+} after calcination. The C2 (IS= 0.34 mm/s, QS= 0.75 mm/s) and

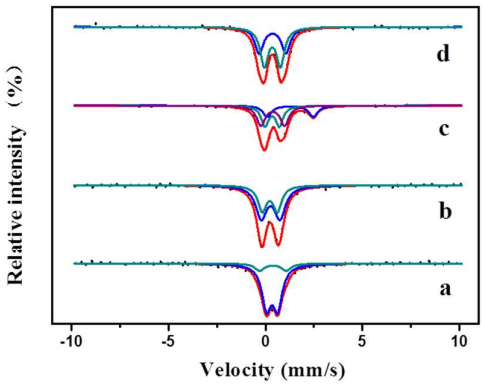

Fig. 6 Mössbauer spectra of (a) as-prepared Fe-Si-1, (b) calcined Fe-Si-1, (c) as-prepared g-Fe-Si-1(2) and (d) calcined g-Fe-Si-1(2) at room temperature

Table 1 Mössbauer fitting parameters of spectra in Fig. 6

Sample	Component	Isomer shift (mm/s)	Quadrupole splitting (mm/s)	Spectral area (%)	Oxidation state
as-prepared Fe-Si-1	A1	0.34	0.58	85.5	Fe^{3+}
	A2	0.38	1.37	14.6	Fe^{3+}
calcined Fe-Si-1	B1	0.26	0.97	62.0	Fe^{3+}
	B2	0.22	0.78	38.0	Fe^{3+}
as-prepared g-Fe-Si-1(2)	C1	1.28	2.37	23.6	Fe^{2+}
	C2	0.34	0.75	35.5	Fe^{3+}
	C3	0.37	1.22	40.9	Fe^{3+}
calcined g-Fe-Si-1(2)	D1	0.35	0.83	57.5	Fe^{3+}
	D2	0.36	1.38	42.5	Fe^{3+}

D1 (IS=0.35 mm/s, QS= 0.83 mm/s) are ascribed to superparamagnetic α-Fe_2O_3 with sizes less than 13.5 nm. Meanwhile, the C3 (IS= 0.37 mm/s, QS= 1.22 mm/s) and D2 (IS= 0.36 mm/s, QS= 1.38 mm/s) are ascribed to Fe^{3+} in a strong distorted octahedral environment, most likely Fe^{3+} oligomeric clusters.[43-45] Indeed, all these results are in excellent agreement with those of the above XPS spectra. Thus, g-Fe-Si-1(2) has been identified as iron-containing MFI zeolite microspheres, which possess evenly dispersed α-Fe_2O_3 nanoparticles.

In conclusion, nanorod-aggregated zeolite microspheres containing iron are prepared through one-step hydrothermal crystallization. The excess iron atoms inhibit the crystallization and reduce the crystallinity. However after adding a small amount of glucose in the synthesis system, iron atoms combine with glucose and are prevented taking part in crystallization of MFI zeolite. In the end, the Fe species convert into the well-dispersed α-Fe_2O_3 nanoparticles in the microspheres. But if adding excess glucose as that in g-Fe-Si-1(4), a large amount of acid produced in the process of crystallization at 170°C.[46] The crystallinity of samples reduced again owing to the change of pH value.

Catalytic tests

Photocatalytic degradation of organic pollutants is becoming one of the most promising green chemistry technologies. The α-Fe_2O_3 (hematite), an environmentally friendly functional material, is extensively used as Fenton-like catalysts in the degradation of organic contaminants such as phenol.[47-49] Hence, MFI zeolite microspheres containing α-Fe_2O_3 nanoparticles was used as catalyst in degradation of phenol. The efficiency of heterogeneous photo-Fenton process was evaluated through chemical oxygen demand (COD). As a comparison, the photocatalytic performance of P25 as a traditional photocatalyst was also evaluated under the same condition. As shown in Fig. 7, it is clearly observed that only g-Fe-Si-1(2) ensures the COD removal rate up to 100% after 90 minutes. Meanwhile, the COD removal rates on P25 and Fe-Si-1 just attain to 29% and 25% after 120 minutes, respectively. The result can be ascribed to low surface area for these two samples, which is disadvantageous for adsorption and diffusion of organic molecules. Moreover, the low catalytic activity on Fe-Si-1 also results from the absence of highly active α-Fe_2O_3 nanoparticles. The initial pH value is a very important factor affecting the Fenton-like processes. A series of photocatalytic reactions were carried out at different pH values and the catalyst g-Fe-Si-1(2) presented the highest COD removal efficiency at pH 3 (Fig.8). While the COD removal rate can finally exceed 90% in a broad pH value range from 2 to 8.

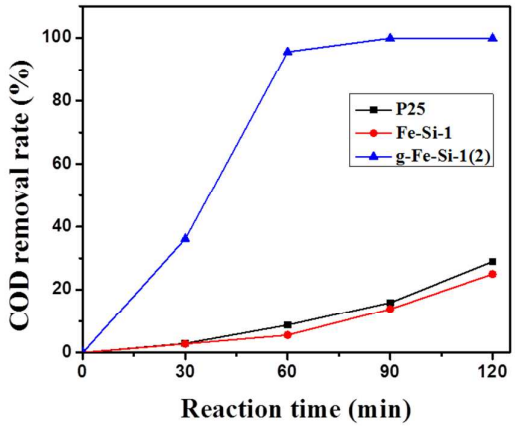

Fig. 7 Photocatalytic degradation of phenol over P25, Fe-Si-1 and g-Fe-Si-1(2) at pH 3

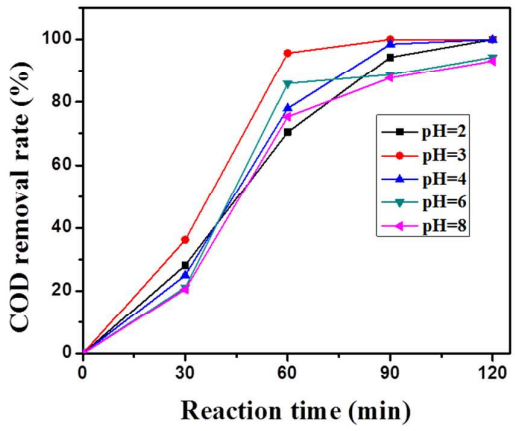

Fig. 8 Effect of initial pH of the solution on phenol degradation over g-Fe-Si-1(2)

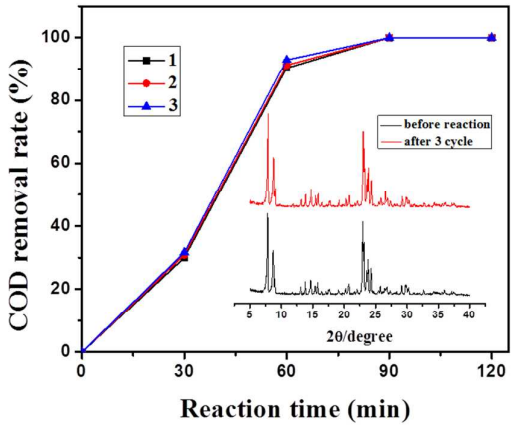

Fig. 9 Recyclability of g-Fe-Si-1(2) for photocatalytic degradation of phenol at pH 3, insert: XRD pattern of fresh and used catalysts

This observation is important since it is well known that one major drawback of homogeneous photo-Fenton is the rigid pH range. The result reveals that it is possible to expand the range of pH values in which Fenton-like processes can occur and no iron hydroxide sludge is formed.

The recyclability is a basic demanded character for a practical solid catalyst. After first-round reaction, the catalyst was separated by centrifugation and washed with deionized water. Then the recovered catalyst was reused in subsequent reaction under the same condition. Finally, the recovered catalyst was examined by powder XRD. As shown in Fig. 9, the catalyst g-Fe-Si-1(2) can keep catalytic activity in 3 cycles and no noticeable loss of the activity is observed. The XRD study reveals that the crystalline structure of recovered catalyst also has no significant change (shown in Fig. 9 inset). All the results indicate that g-Fe-Si-1(2) is an excellent catalyst for photocatalytic degradation of phenol, owing to its hierarchically porous, high surface area, evenly dispersed α-Fe_2O_3 nanoparticles and good reusability.

Conclusions

In summary, hierarchical iron-containing MFI zeolite microspheres with nanorod oriented-assembled structures have been successfully synthesized by one-step hydrothermal crystallization without mesoporous template agent. After adding a certain amount of glucose in synthetic system, the obtained samples possess a relatively uniform spherical morphology (4-5μm), hierarchical porous, high surface area and ultrafine α-Fe_2O_3 nanoparticles. In the process, glucose plays an important role on the iron species and crystallinity of zeolite microspheres. Moreover, the obtained microspheres show excellent catalytic performance for photocatalytic degradation of phenol. Additionally, this catalyst has good stability and can keep the good photo-Fenton performance after multiple cycles, implying that it has great potential in the treatment of agro-industrial wastewater. This synthesis method overcomes the disadvantages of multistep synthesis and post-processing methods. The approach opens up routes for the in-situ preparation of other functional porous materials with unique nanostructure.

Acknowledgements

The authors acknowledge the financial support from the Program for New Century Excellent Talents in University (NCET-04-0270).

Notes and references

1 J. Weitkamp, Solid State Ionics, 2000, **131**, 175-188.
2 A. Corma, *Chem. Rev.*, 1997, **97**, 2373-2420.
3 M. E. Davis, *Nature*, 2002, **417**, 813-821.
4 C. S. Cundy and P. A. Cox, *Chem. Rev.*, 2003, **103**, 663-702.
5 B. Zhu, L. Zou, C. M. Doherty, A. J. Hill, Y. Lin, X. Hu, H. Wang and M. Duke, *J. Mater. Chem.*, 2010, **20**, 4675-4683.
6 F. Xu, Y. Wang, X. Wang, Y. Zhang, Y. Tang and P. Yang, *Adv. Mater.*, 2003, **15**, 1751-1753.
7 L. Tosheva, V. Valtchev and J. Sterte, *Microporous Mesoporous Mater.*, 2000, **35**, 621-629.
8 V. Naydenov, L. Tosheva and J. Sterte, *Chem. Mater.*, 2002, **14**, 4881-4885.
9 Y. Kang, W. Shan, J. Wu, Y. Zhang, X. Wang, W. Yang and Y. Tang, *Chem. Mater.*, 2006, **18**, 1861-1866.
10 J. Hua and Y. Han, *Chem. Mater.*, 2009, **21**, 2344-2348.
11 J. Zhao, J. Zhou, Y. Chen, Q. He, M. Ruan, L. Guo, J. Shi and H. Chen, *J. Mater. Chem.*, 2009, **19**, 7614-7616.
12 H. Tao, H. Yang, Y. Zhang, J. Ren, X. Liu, Y. Wang and G. Lu, *J. Mater. Chem. A.*, 2013, **1**, 13821-13827.
13 Z. Wang, J. Guan, S. Wu, C. Xu, Y. Ma, J. Lei and Q. Kan, *Mater. Lett.*, 2010, **64**, 1325-1327.
14 C. Yin, D. Tian, M. Xu, Y. Wei, X. Bao, Y. Chen and F. Wang, *J. Colloid. Interface. Sci.*, 2013, **397**, 108-113.
15 B. Li, B. Sun, X. Qian, W. Li, Z. Wu, Z. Sun, M. Qiao, M. Duke and D. Zhao, *J. Am. Chem. Soc.*, 2013, **135**, 1181-1184.
16 R. Prihod'ko, I. Stolyarova, G. Gündüz, O. Taran, S. Yashnik, V. Parmon and V. Goncharuk, *Appl. Catal. B: Environ.*, 2011, **104**, 201-210.
17 S. Navalon, M. Alvaro and H. Garcia, *Appl. Catal. B: Environ.*, 2010, **99**, 1-26.
18 K. Jíša, J. Nováková, M. Schwarze, A. Vondrová, S. Sklenák and Z. Sobalik, *J. Catal.*, 2009, **262**, 27-34.
19 M. Choi, Z. Wu and E. Iglesia, *J. Am. Chem. Soc.*, 2010, **132**, 9129-9137.
20 A. B. Laursen, K. T. Højholt, L. F. Lundegaard, S. B. Simonsen, S. Helveg, F. Schüth, M. Paul, J. D. Grunwaldt, S. Kegnæs and C. H. Christensen, *Angew. Chem. Int. Ed.*, 2010, **122**, 3582-3585.
21 K. Scholle, W. Veeman, P. Frenken and G. Van der Velden, *Appl. Catal.*, 1985, **17**, 233-259.
22 J. Jansen, F. Van der Gaag and H. Van Bekkum, *Zeolites*, 1984, **4**, 369-372.
23 D. B. Shukla and V. P. Pandya, *J. Chem. Techol. Biot.*, 1989, **44**, 147-154.
24 S. Bordiga, R. Buzzoni, F. Geobaldo, C. Lamberti, E. Giamello, A. Zecchina, G. Leofanti, G. Petrini, G. Tozzola and G. Vlaic, *J. Catal.*, 1996, **158**, 486-501.
25 E. Hensen, Q. Zhu, R. Janssen, P. Magusin, P. Kooyman and R. Van Santen, *J. Catal.*, 2005, **233**, 123-135.
26 M. Schwidder, M. S. Kumar, K. Klementiev, M. M. Pohl, A. Brückner and W. Grünert, *J. Catal.*, 2005, **231**, 314-330.

27 A. Koekkoek, W. Kim, V. Degirmenci, H. Xin, R. Ryoo and E. Hensen, *J. Catal.*, 2013, **299**, 81-89.
28 H. Zhang, H. Ming, S. Lian, H. Huang, H. Li, L. Zhang, Y. Liu, Z. Kang and S.-T. Lee, *H. Zhang, H. Ming, S. Lian, H. Huang, H. Li, L. Zhang, Y. Liu, Z. Kang and S.-T. Lee, Dalton Trans.*, 2011, **40**, 10822-10825.
29 M. Noorjahan, V. Durga Kumari, M. Subrahmanyam and L. Panda, *Appl. Catal. B: Environ.*, 2005, **57**, 291-298.
30 S. Roosendaal, B. Van Asselen, J. Elsenaar, A. Vredenberg and F. Habraken, *Surf. Sci.*, 1999, **442**, 329-337.
31 P. C. Graat and M. A. Somers, *Appl. Surf. Sci.*, 1996, **100**, 36-40.
32 S. Shwan, R. Nedyalkova, J. Jansson, J. Korsgren, L. Olsson and M. Skoglundh, *Ind. Eng. Chem. Res.*, 2012, **51**, 12762-12772.
33 P. Sazama, N. K. Sathu, E. Tabor, B. Wichterlová, Š. Sklenák and Z. Sobalík, *J. Catal.*, 2013, **299**, 188-203.
34 K. Dubkov, N. Ovanesyan, A. Shteinman, E. Starokon and G. Panov, *J. Catal.*, 2002, **207**, 341-352.
35 K. Lázár, G. Lejeune, R. Ahedi, S. Shevade and A. Kotasthane, *J. Phys. Chem. B.*, 1998, **102**, 4865-4870.
36 G. Fierro, G. Moretti, G. Ferraris and G. B. Andreozzi, *Appl. Catal. B: Environ.*, 2011, **102**, 215-223.
37 A. Meagher, V. Nair and R. Szostak, *Zeolites*, 1988, **8**, 3-11.
38 R. Garten, W. Delgass and M. Boudart, *J. Catal.*, 1970, **18**, 90-107.
39 D. M. Kurtz Jr, *Chem. Rev.*, 1990, **90**, 585-606.
40 K. Dubkov, N. Ovanesyan, A. Shteinman, E. Starokon and G. Panov, *J. Catal.*, 2002, **207**, 341-352.
41 K. Lázár, G. Borbély and H. Beyer, Zeolites, 1991, **11**, 214-222.
42 J. Pérez-Ramırez, G. Mul, F. Kapteijn, J. Moulijn, A. Overweg, A. Doménech, A. Ribera and I. Arends, *J. Catal.*, 2002, **207**, 113-126.
43 M. Iwasaki, K. Yamazaki, K. Banno and H. Shinjoh, *J. Catal.*, 2008, **260**, 205-216.
44 A. Battiston, J. Bitter, F. De Groot, A. Overweg, O. Stephan, J. Van Bokhoven, P. Kooyman, C. Van Der Spek, G. Vanko and D. Koningsberger, *J. Catal.*, 2003, **213**, 251-271.
45 E. Hensen, Q. Zhu, M. Hendrix, A. Overweg, P. Kooyman, M. Sychev and R. Van Santen, *J. Catal.*, 2004, **221**, 560-574.
46 X. Sun and Y. Li, Angew. Chem. Int. Ed., 2004, 43, 597-601.
47 M. Valenzuela, P. Bosch, J. Jiménez-Becerrill, O. Quiroz and A. Páez, *J. Photoch. Photobio. A.*, 2002, **148**, 177-182.
48 S.-W. Cao, Y.-J. Zhu, G.-F. Cheng and Y.-H. Huang, *J. Phy. Chem. Solids.*, 2010, **71**, 1680-1683.
49 Q. Sun, W. Leng, Z. Li and Y. Xu, *J. Hazard. Mater.*, 2012, **229**, 224-232.

Graphical abstracts

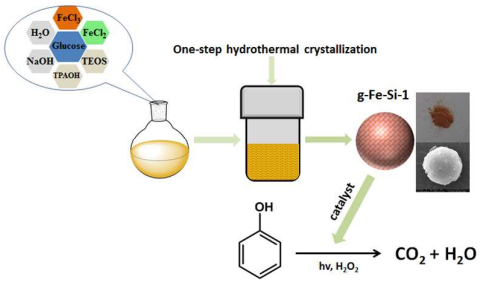

The hierarchical iron-containing MFI zeolite microsphere was prepared and investigated as heterogeneous Fenton-like catalyst for photocatalytic degradation of phenol.